Earth, Planets and Space

TECHNICAL REPORT

Open Access

Energetic particle flux measurements from the Korean space weather monitor particle detector: a comparative study with the MPS-HI onboard GOES-16

Daehyeon Oh[1], Jiyoung Kim[1*], Paul T. M. Loto'aniu[2,3], Han-Cheol Lim[1], Dae-Young Lee[4] and Dohyeong Kim[1]

Abstract

The Korean space weather monitor (KSEM) aboard the GEO-KOMPSAT-2A (GK2A) has been continuously measuring energetic particle flux in geostationary orbit at 128.2°E longitude since July 2019. The particle detector (PD) component of KSEM comprises six particle telescopes viewing different directions that provide near-real-time electron flux observations within the energy range of 100 keV to 3.8 MeV. The KSEM PD on the GK2A satellite, together with the MPS-HI on the GOES-16 satellite 156.6° away, can provide valuable simultaneous observations of the asymmetric space environment and contributes to our understanding of this dynamic region. In this study, we present recent energetic electron flux measurements obtained from the KSEM PD and conduct preliminary cross-comparisons with data from the Magnetosphere Particle Sensor–High (MPS-HI) PD, which is part of the SEISS instrument suite onboard GOES-16. The inter-comparisons show that the electron fluxes of the two detectors are in reasonable similarity except for some energy bands under quiet conditions. Additionally, we provide a brief overview of the electron flux responses of both KSEM PD and MPS-HI under enhanced space environment conditions, which shows differences based on sensor characteristics and satellite location.

Keywords Space weather, In situ measurement, Energetic particle, High-energy electron, High-energy proton, Geostationary orbit, Inter-comparison

*Correspondence:
Jiyoung Kim
aceasia@korea.kr
Full list of author information is available at the end of the article

Graphical Abstract

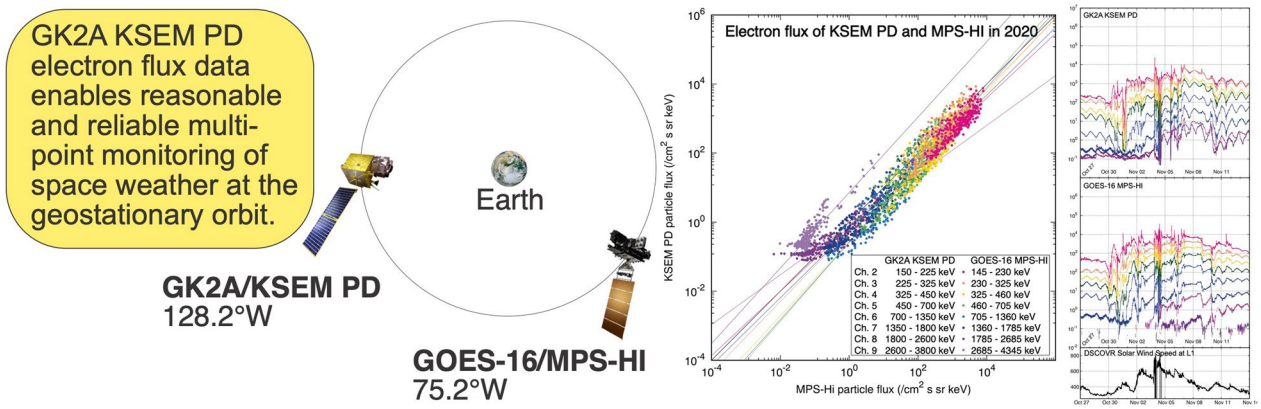

Background

The geostationary Earth orbit (GEO) is an ideal location for satellites, including telecommunications, broadcasting, and weather monitoring, as it provides a constant view of a fixed region on the Earth's surface. However, the GEO is also subject to dynamic space weather phenomena that can impact satellites. Satellites in GEO, expected to have an operational lifetime of ≥ 10 years, are more vulnerable to extreme space weather events, such as strong magnetic storms or solar energetic particle events, which can cause malfunctions, data loss, and communication disruptions (Choi et al. 2011; Lohmeyer and Cahoy 2013). In particular, energetic particle exposures could increase satellite operational anomalies (Baker 2001). Thus, monitoring energetic particle fluxes is crucial for ensuring the operational longevity of satellites in the GEO.

Satellite-based in situ observations of the near-Earth space environment have significantly advanced our understanding of space weather phenomena. Since the launch of the Explorer 1 satellite, which discovered the Van Allen radiation belts (Allen et al. 1958), many satellite-based space physics/space weather missions have been launched (e.g., MAGSAT, CHAMP, and POLAR). Some of the longest continuous monitoring of the near-Earth space energetic particle environment has come from the Los Alamos National Laboratory satellite measurements from 1989 to 2016 and from the National Oceanic and Atmospheric Administration (NOAA) Geostationary Operational Environmental Satellite (GOES) series, which has operated the Space Environment Monitor (SEM) on SMS (The Synchronous Meteorological Satellites) and GOES since 1974. Recently, NOAA launched three GOES-R series satellites (GOES-16, GOES-17, and GOES-18), including the particle sensor suite named the Space Environment in situ Suite (Dichter et al. 2015), and other space weather instruments. Japan Meteorological Agency (JMA) is operating geostationary meteorological satellites Himawari-8 and -9, which include a space environment data acquisition monitor (Bessho et al. 2016). China Meteorological Administration (CMA) has launched the geostationary satellite Fengyun (FY)-2 and FY-4 series, which include a SEM suite and a space environment package as a payload (Yang et al. 2016). In addition, the European Space Agency (ESA) has deployed the Next Generation Radiation Monitor (NGRM) unit on the European Data Relay System, Satellite-C (EDRS-C) to monitor space radiation (Sandberg et al. 2022).

The Korea Meteorological Administration launched the GEO-KOMPSAT-2A (GK2A) satellite on December 4, 2018, which features the Korean space weather monitor (KSEM) as a secondary payload (Oh et al. 2018). The KSEM mission aims to provide real-time in situ monitoring of space weather from the GEO at a longitude of 128.2°E. The KSEM instrument suite includes the KSEM particle detector (PD), a magnetometer, and a charging monitor (Magnes et al. 2020; Seon et al. 2020; Woo et al. 2020).

This study presents initial electron flux observations at geostationary altitude made by the KSEM PD, along with preliminary cross-comparisons with data from the Magnetosphere Particle Sensor–High (MPS-HI) (Dichter et al. 2015) on the GOES-16 satellite. The GOES-16 satellite operates in GEO at a longitude of 75.2°W, a position that is 156.6° (equivalent to 10 h 26 min in local time) away from GK2A, almost on the

opposite side of the Earth. This positioning of the satellites allows for simultaneous observations of the same space weather phenomena from different locations, thereby providing a more comprehensive coverage of the space environment. The electron channel energies of KSEM PD and MPS-HI are shown in Table 1.

Instruments overview

The KSEM PD inherits its fundamental design and structure from satellite-based particle sensors on WIND, STEREO, THEMIS, and MAVEN (Lin et al. 1995; Luhmann et al. 2005; Sibeck and Angelopoulos 2008; Larson et al. 2015). It has been modified to improve the detectable particle energy range by increasing the number and thickness of detectors. Figure 1 presents illustrations of the KSEM PD and GK2A. The KSEM PD consists of three independent units of identical design and structure, PD1, PD2, and PD3. Each unit consists of a pair of identical double-ended heads solid-state telescopes (SSTs) to detect electrons and protons from opposite directions with a 20×20° field of view. In total, the KSEM PD comprises six electron telescopes, each providing a different viewing direction. Figure 2 and Table 2 provide the boresight directions of KSEM PD telescopes.

The KSEM PD's detectable energy range is 100 keV–3.8 MeV, which is particularly important for monitoring space weather phenomena and their impacts on GEO satellites. Significant internal charging of satellites is usually associated with electron fluxes of 100 keV–3 MeV (NASA 2011), which can infiltrate the satellite and increase the potential for electrostatic discharge (Ferguson et al. 2011). Moreover, increases in the 200 keV–1.5 MeV electron fluence, especially, can elevate the likelihood of anomalies in geostationary satellites (Sakaguchi and Nagatsuma 2022). In the recent critical satellite anomaly, (Loto'aniu et al. 2015) showed a flux of 75–475 keV electrons, the highest to date since 2009, when the Galaxy 15 geostationary satellite experienced a loss of control and stopped responding to the ground on April 5, 2010. In contrast, the fluxes of higher-energy electrons (>0.8 MeV) and protons (>6.5 MeV) did not show any significant increase.

Table 1 Energies of KSEM PD and MPS-HI electron channels

Channel No	KSEM PD energy (keV)	MPS-HI energy (keV)
1	100–150	90–145
2	150–225	145–230
3	225–325	230–325
4	325–450	325–460
5	450–700	460–705
6	700–1350	705–1360
7	1350–1800	1360–1785
8	1800–2600	1785–2685
9	2600–3800	2685–4345
10	2000–3800	>2000 (integral)

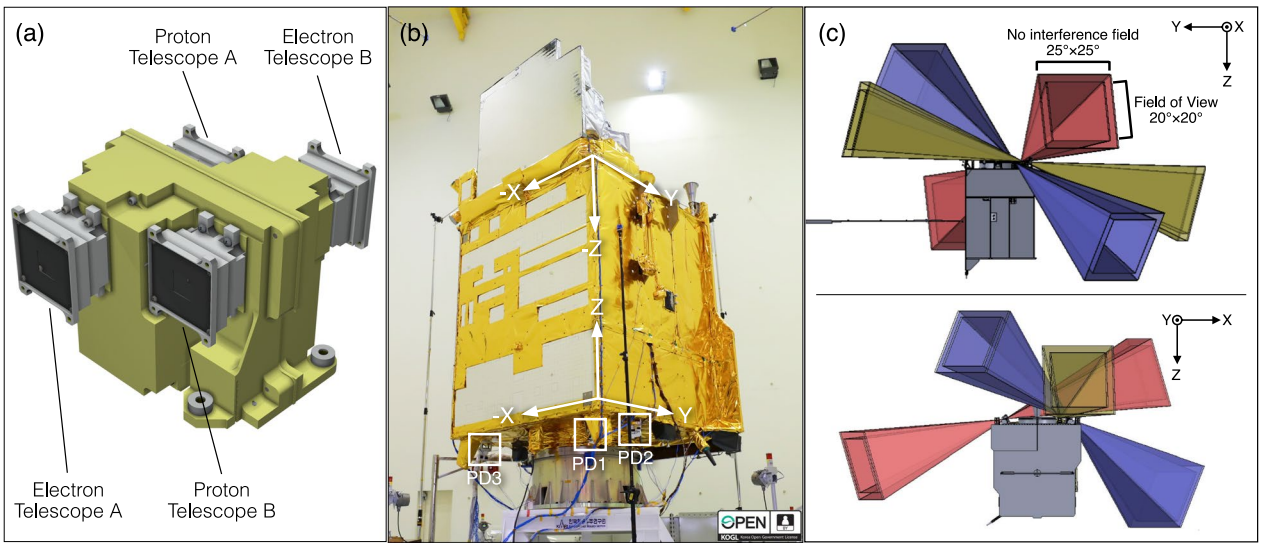

Fig. 1 KSEM PD and GK2A satellite. **a** Configuration of the KSEM PD. **b** Location of KSEM PD units. PD1, PD2 and PD3 are mounted on the underside of the GK2A satellite, facing away from Earth. The X, Y, and Z axes correspond to the east (the satellite's velocity direction), south, and nadir direction (the Earth's direction), respectively. Each coordinate axis in the figure aligns parallel to the edges of the spacecraft. The original image is a public work of the Korea Aerospace Research Institute and is used according to the Korea Open Government License Type 1. **c** Illustration of field of views for PD telescopes

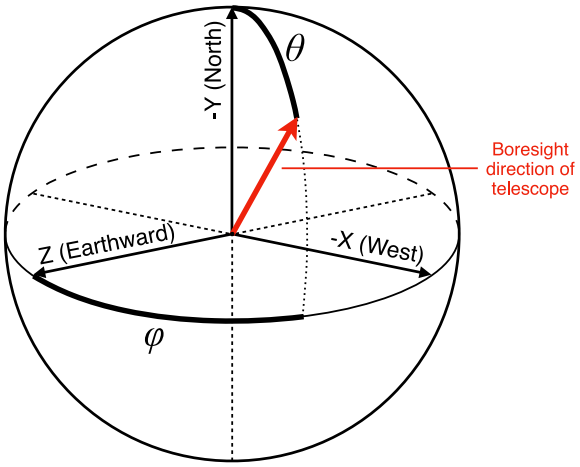

Fig. 2 The definition of angular variables for boresight directions of PD telescopes. The specific boresight directions for each telescope are listed in Table 2

Table 2 The boresight directions of each PD telescope

Electron telescope	θ (°)	φ (°)
PD1 Telescope A	15	25
PD1 Telescope B	165	205
PD2 Telescope A	51	308
PD2 Telescope B	129	128
PD3 Telescope A	109	72
PD3 Telescope B	71	252

The definition of angular variables is shown in Fig. 2

The KSEM PD has been successfully deployed and commissioned to make reliable measurements of the energetic particle population at its location. (Seon et al. 2020) demonstrated that its instruments are operational and can provide serviceable inputs to space science and space weather communities. It is worth noting that the lowest energy channel (Channel 1: 100–150 keV) was not used in this study, as it is currently undergoing additional calibration to optimize and improve the status of each telescope. For more detailed and technical descriptions of KSEM PD, refer to Seon et al. (2020).

Cross-comparison between KSEM PD and MPS-HI

The KSEM PD has six telescopes, while MPS-HI has five telescopes, two and three of which operate in different energy ranges. In the case of MPS-HI, we used telescopes 1, 2, and 4, which operate in the same energy ranges. Since no pair of telescopes from both satellites has a similar viewing direction, we considered omnidirectional fluxes in this work. These fluxes are calculated by averaging all directional flux densities. Comparing omnidirectional fluxes from two different sensors with limited fields of view may introduce some variance due to the different observing geometries of the telescopes. However, the goal of this work is to provide practical data that can be readily used in real-time space weather monitoring and forecasting systems. In this context, omnidirectional fluxes serve effectively as they represent a standard and commonly used measure. This approach provides us with a practical and robust method to obtain comparable measurements.

We analyzed two years of data from 2020 and 2021. Figure 3 displays the geomagnetic status during this period using geomagnetic indices (Kp and Dst). The start of 2020 coincided with the minimum phase of solar cycle 25 from December 2019, characterized by weaker solar activities and lower occurrence rates of significant space weather events than previous solar cycles. In 2020, the geomagnetic activity was mostly weak, with Kp < 4 and Dst > − 40 nT, except for a few multi-days disturbances. In 2021, generally weak geomagnetic conditions prevailed although these indices sometimes exceeded 4 and − 40 nT, respectively, including a strong disturbance in May and November with *K*p over 7. Because of the limited occurrence and relatively short duration of active conditions, the impact of these magnetic disturbances may not be significant in long-term analyses. However, to mitigate any potential influence, we have selected magnetically quiet days, defined as those with a daily average Kp index of 2 or less. In 2020, 321 out of 366 days met this condition, and in 2021, 274 out of 365 days also satisfied this criterion.

Figure 4 displays the time series of electron flux data for KSEM PD and MPS-HI from 2020 to 2021. It presents an overview of the long-term data trends observed from the two satellites. Despite some differences in detail, which may be due to location or sensor differences, the electron flux measurements from both detectors showed good agreement on a two-year timescale. MPS-HI showed a slightly higher flux during the enhancement phases than KSEM PD from Channels 2 to 7. However, this trend was reversed during prolonged minor geomagnetic storms in August–September 2020 and March 2021. In Channels 8 and 9, the two detectors showed a constant background offset, with KSEM PD measuring higher fluxes than MPS-HI. This offset can be attributed to certain intrinsic aspects of their respective algorithms. The algorithm applied to the GOES-16 MPS-HI electron telescope includes a step to eliminate background noise caused by proton contamination. This is achieved using the 80–500 MeV proton flux data, as described in Galica et al. (2016). This may explain the differences observed in channels 8 and 9.

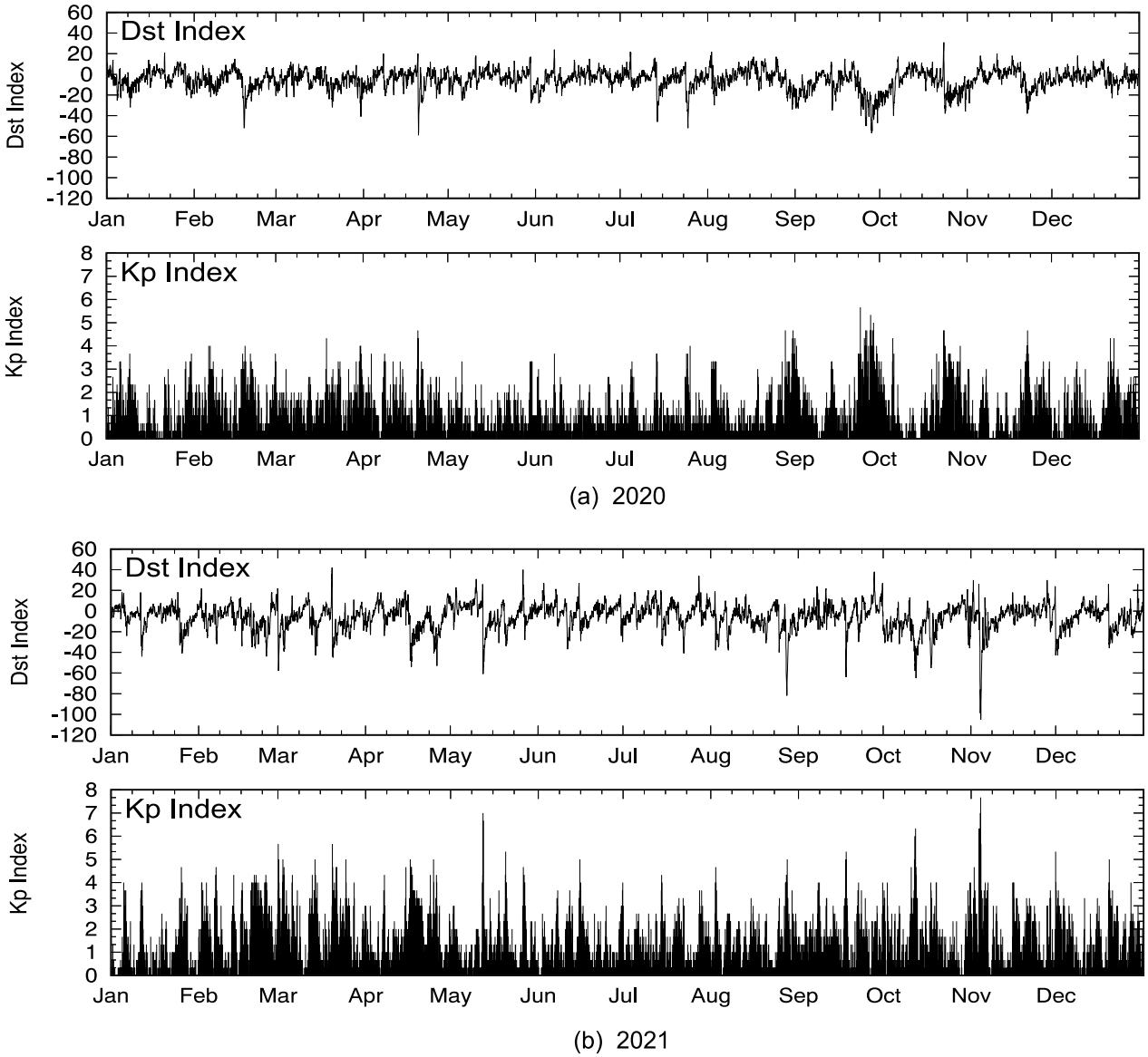

Fig. 3 Geomagnetic indices (Kp and Dst). The period was characterized by low solar activity during the solar minimum between cycles 24 and 25, with relatively low geomagnetic activity

Figure 5 shows scatter plots of a daily average electron particle flux on magnetically quiet days ($Kp \leq 2$) with a conjunction condition of $dL^* < 0.1$ between the two satellites, and L^* was calculated using the OP77 quiet day model in SpacePy 0.0.2 (Burrell et al. 2018; Morley et al. 2022). Flux averaging was performed exclusively during periods that met the conjunction condition; subsequently, the results were further averaged on a daily basis. The local times of the two satellites and the number of data points, satisfying the conjunction condition of $dL^* < 0.1$, are provided in Additional file 1 and Additional file 2. While we employed static magnetic field models, the matching time ranges shift gradually, attributed to the Earth's revolution, altering the relative orientation of its axis with respect to the Sun. The result shows a reasonable correlation for most channels, except for Channel 9. The Pearson's R values of the logarithms, obtained from $\log(\mathrm{Flux}_{[\mathrm{KSEM\ PD}]}) = \alpha \log(\mathrm{Flux}_{[\mathrm{MPS\text{-}HI}]}) + \beta$, are shown in Table 3, including slope α and intercept β of the fitting lines. The R values were ~ 0.85 or greater, indicating a strong correlation between the data from the two detectors. For channels 7 and 8, the data points are slightly curved at the bottom. This is a reflection of the different detection limits of the two instruments, which is

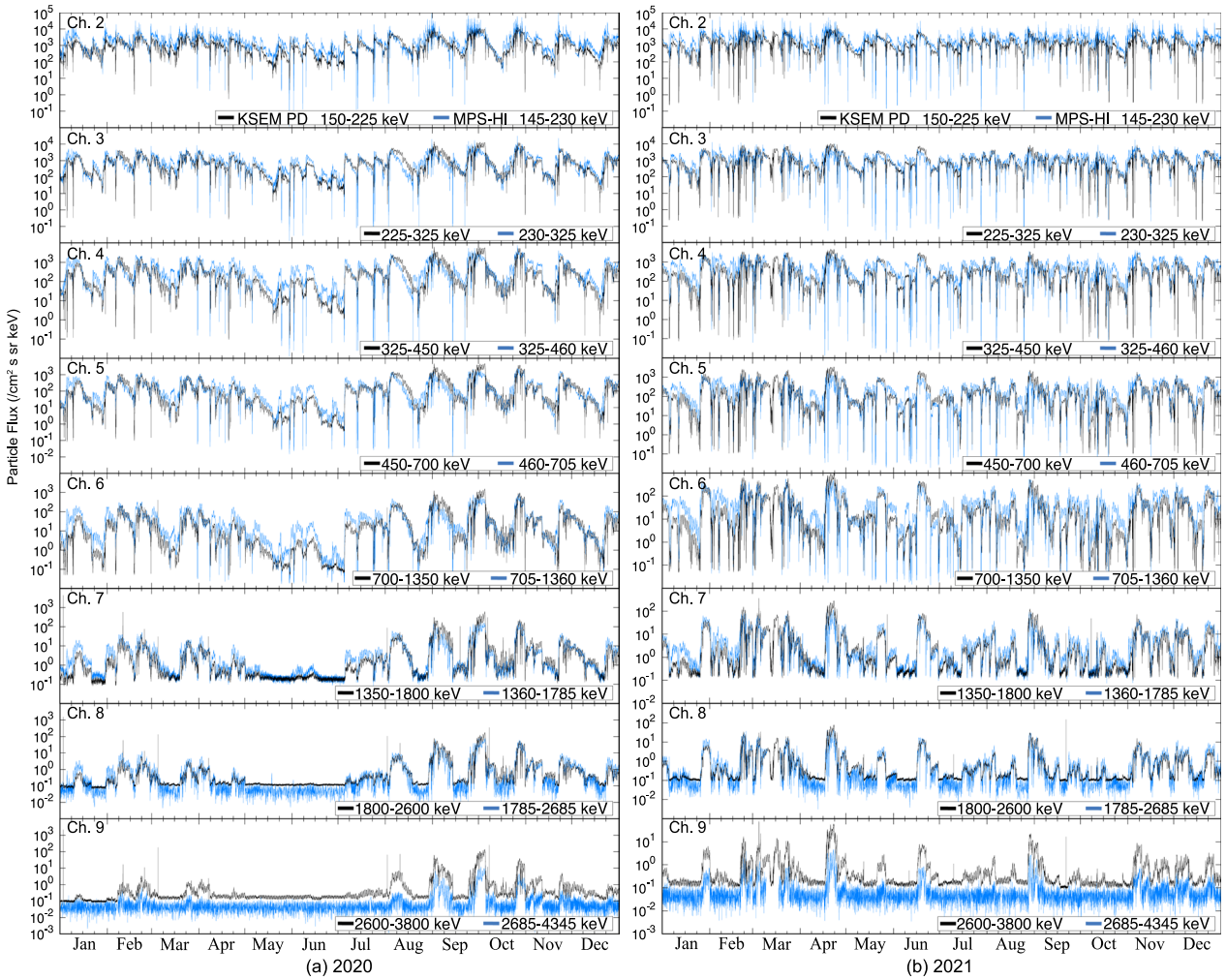

Fig. 4 Time series of electron flux data comparison between KSEM PD and MPS-HI, 2020–2021. Good correspondence was observed, with slight flux variation during enhancements and geomagnetic storms. An offset observed in Channels 8 and 9, with KSEM PD showing higher flux

common when comparing data from two different instruments (e.g., Zhang et al. 2018).

Figure 6 presents flux-energy spectra on days with $Kp \leq 2$ and $dL^* < 0.1$, in the years 2020 and 2021. Figure 6a shows that the energy spectra of the KSEM PD and MPS-HI fluxes are in good agreement with similar spectral shapes, except for Channel 2, 4 and 9. We used the nominal energies from MPS-HI as described in the "GOES-R Series Data Book" (Revision A, May 2019). However, we note that the effective energies obtained from bowtie analysis might slightly vary (Boudouridis et al. 2020). For reference, in Fig. 6a, we added spectra with the bowtie center energies of MPS-HI from Boudouridis et al. 2020. The cause for the slightly lower observed values in KSEM PD's Channel 2 and 4 remains unclear, but we anticipate that future research will offer further clarification on this issue. Figure 6b compares the quarterly spectral flux distributions of both detectors in 2020 and 2021, with each quarter defined as Q1: Jan–Mar, Q2: Apr–Jun, Q3: Jul–Sep, and Q4: Nov–Dec. Despite the similar yearly distributions shown in Fig. 6a, b indicates that KSEM PD had a broader variation in flux density among quarters than MPS-HI. Figure 6c compares the quarterly flux distributions of the two detectors for 2020 and 2021. The variation in 2021 was narrower than in 2020, and the overall flux densities were higher than those in 2020. These characteristics, observed in data from both detectors, may be due to the end of the solar cycle minimum and the gradual increase in solar activity from early 2021.

Figure 7 shows the monthly R values, slope α, and intercept β of the fitting lines, from 2020 to 2021, which generally illustrate reasonable correlations, with occasional exceptions observed in the higher energy ranges. The α values are relatively consistent over time for most

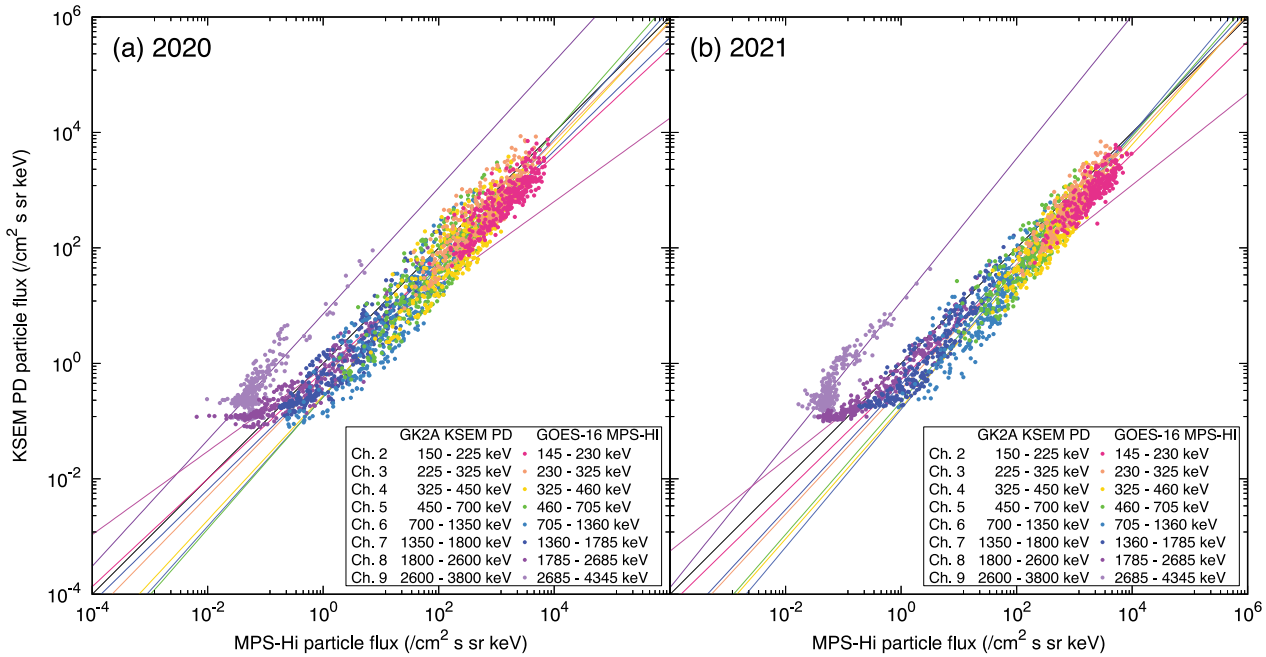

Fig. 5 Scatter plot of a daily average electron particle flux from KSEM PD and MPS-HI, satisfying $dL^* < 0.1$, on magnetically quiet days with average Kp index ≤ 2. The correlation between the data from the two detectors was strong, except for Channel 9. The curves near the bottom of channels 7 and 8 is a reflection of the different detection limits

Table 3 Yearly R values, slope α, and intercept β of the logarithms obtained from $\log(\text{Flux}_{[\text{KSEM PD}]}) = \alpha \log(\text{Flux}_{[\text{MPS-HI}]}) + \beta$

Channel no.	α		β		R	
	2020	2021	2020	2021	2020	2021
2	0.933	0.976	− 0.137	− 0.280	0.867	0.870
3	1.025	1.081	− 0.251	− 0.448	0.878	0.881
4	1.080	1.138	− 0.556	− 0.764	0.874	0.880
5	1.144	1.149	− 0.583	− 0.665	0.903	0.881
6	1.119	1.193	− 0.585	− 0.797	0.924	0.885
7	0.978	1.083	− 0.234	− 0.366	0.935	0.938
8	0.721	0.792	− 0.083	− 0.081	0.925	0.958
9	1.093	1.238	0.856	1.072	0.882	0.899

channels. In channels 7, 8, and 9, notable decreases in R and α values occurred in May and June 2020, as well as in July and October 2021. This decrease is attributed to the fact that there were no significant variations in electron flux within those energy bands and months, thus they are deemed meaningless.

Responses to enhanced energetic particle conditions

Figure 8 shows the observations of three enhanced energetic electron environments by KSEM PD and MPS-HI in 2021. April 14–28 (Case 1), June 13—26 (Case 2), and

(See figure on next page.)

Fig. 6 Energy-based spectral flux distributions with $dL^* < 0.1$ on magnetically quiet days with average Kp index ≤ 2. **a** Spectral flux distributions for 2020 and 2021 showed good agreement between KSEM PD and MPS-HI, with similar power law distributions, except for Channel 9. The effective energy (E_{eff}) of GOES-16 MPS-HI electron channels, as determined by Boudouridis et al. (2020), is also included. **b** Quarterly spectral flux distributions show broader quarterly variation in flux density in KSEM PD, compared with MPS-HI. **c** Comparisons of the quarterly flux distributions of the two detectors showed narrower variation and higher overall flux in 2021

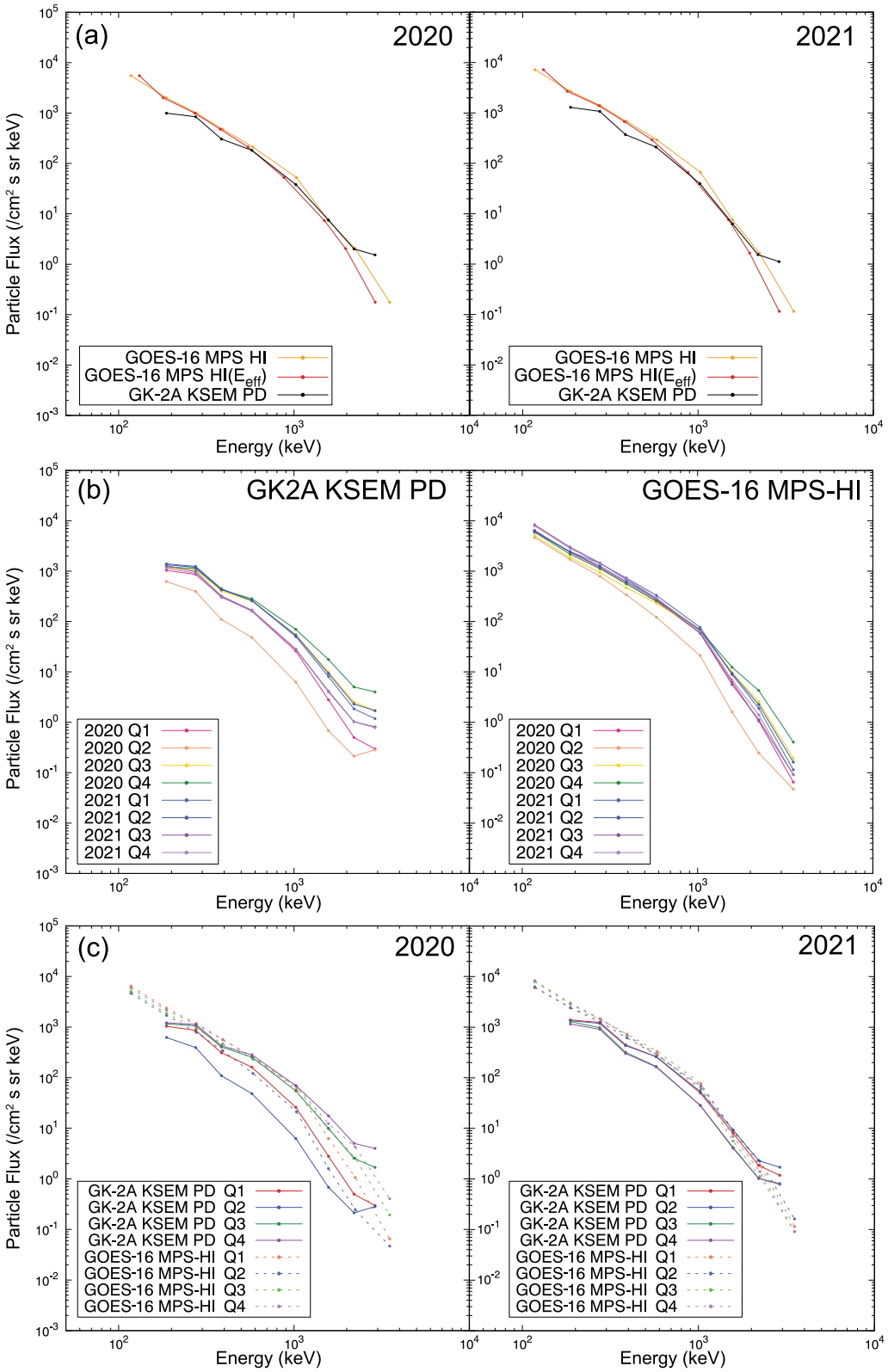

Fig. 6 (See legend on previous page.)

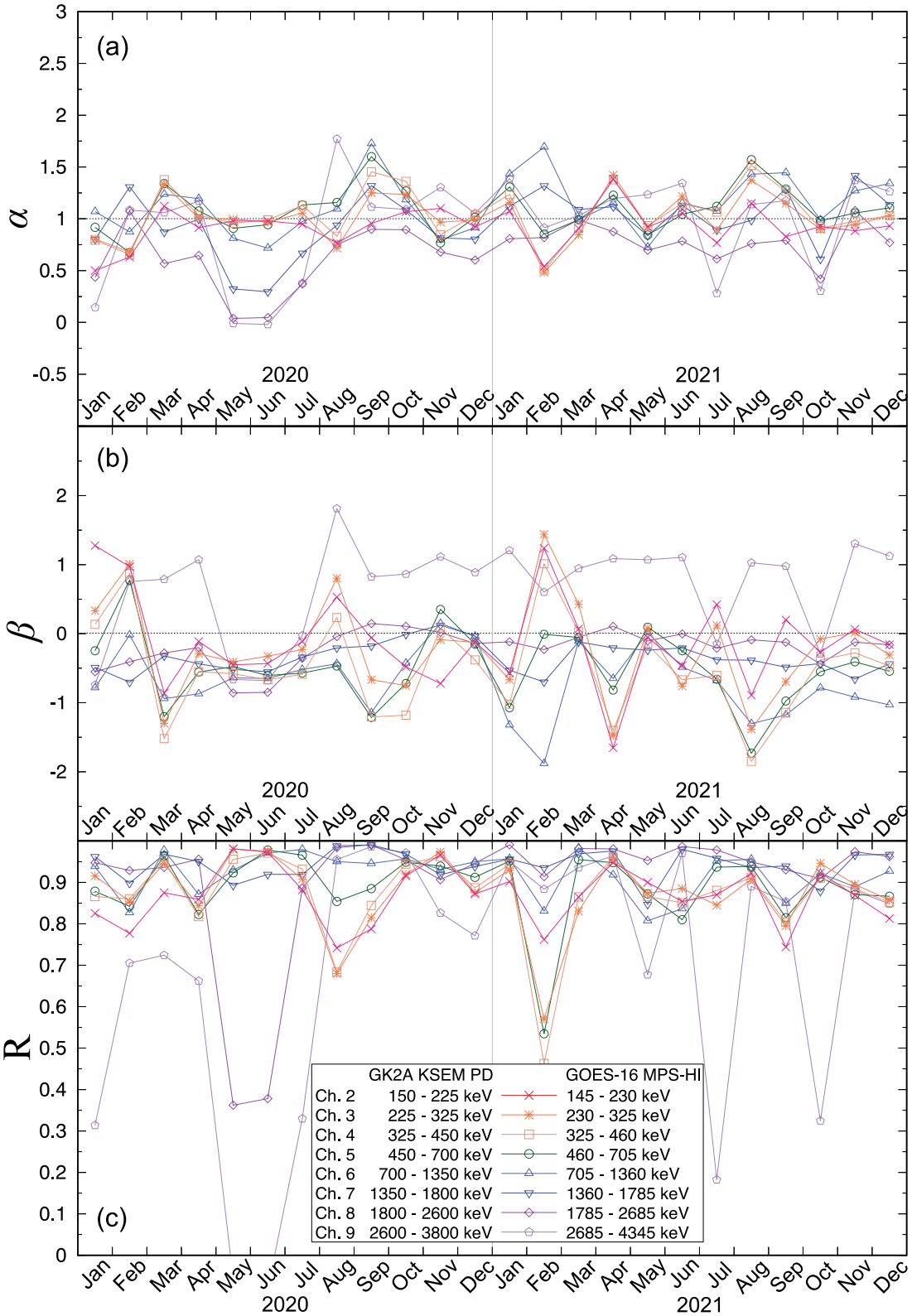

Fig. 7 Monthly R values, slope *α*, and intercept *β* of KSEM PD and MPS-HI data from 2020 to 2021. While there are occasional variations, the R and α values are relatively consistent over time for most channels. Notable decreases in *R* and *α* values above channel 7 during specific months result from the lack of significant flux variation within those energy bands during those time periods

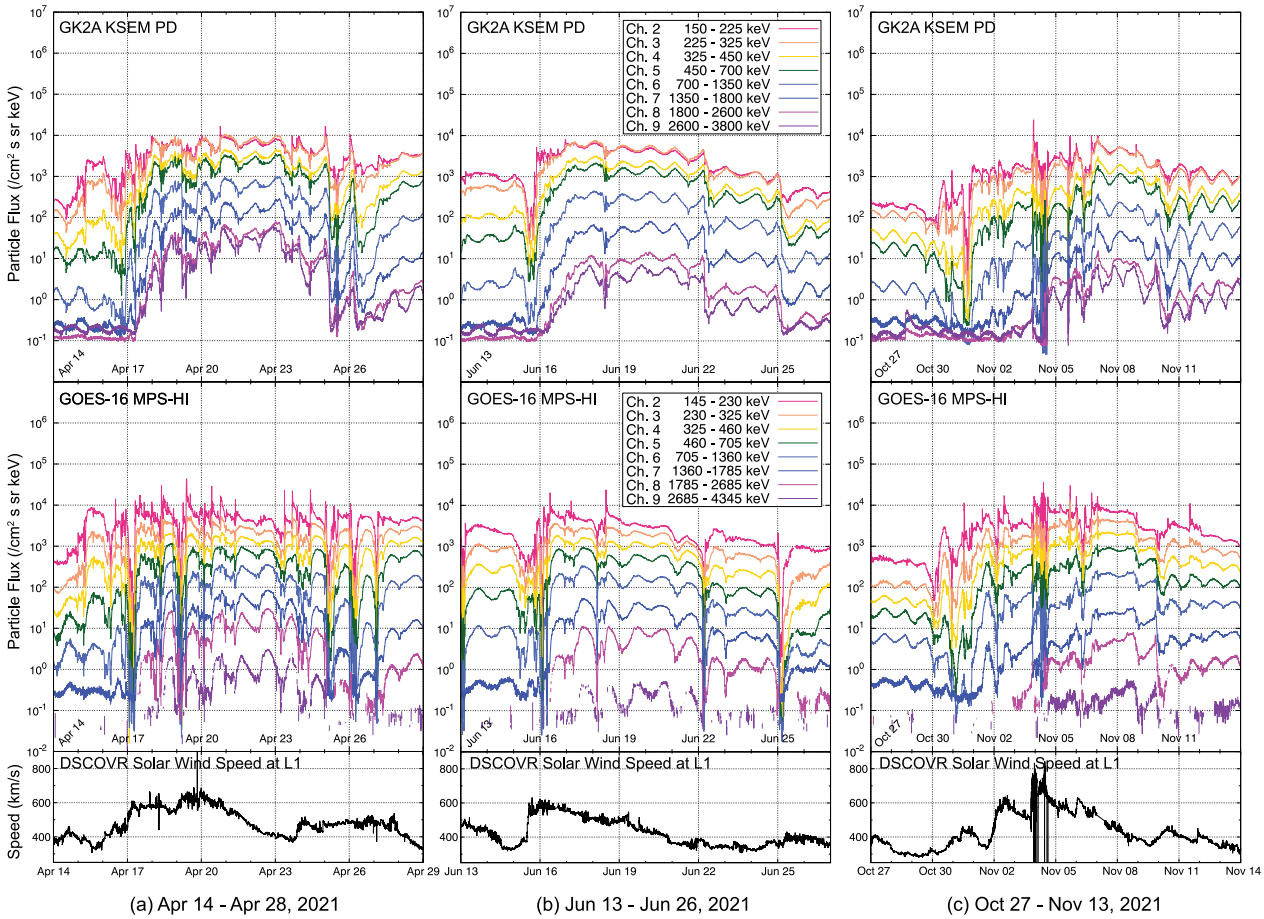

Fig. 8 KSEM PD and MPS-HI electron flux measurements and solar wind speed data from DSCOVR. Point L1 was chosen for observation. Three enhanced space weather cases were selected: **a** April 14–28, **b** June 13–26, and **c** October 27–November 13

October 27—November 13 (Case 3) were selected as they caused relatively higher particle fluxes.

Case 1: April 14–28

In April 2021, a large corona hole faced Earth, resulting in high-speed solar wind streams (HSSs) impacting Earth's magnetosphere starting April 16th. Both KSEM PD and MPS-HI measurements showed enhancements. MPS-HI observed more significant fluctuations during substorms, particularly at the beginning and end of the HSS period. Prior to HSS arrival, the electron fluxes in Channel 9 (2600–3800 keV) and other MeV channels of the KSEM PD had daily variations peaking around 18:00 UT (02:33 MLT), while other lower energy channels peaked near the local noon (12:00 MLT) of the GK2A satellite. After HSS arrival and a weak magnetic storm (Dst index of – 54 nT), electron flux variations in Channel 9 became in-phase with other channels. This shift in electron flux variation was similar to what Nagatsuma et al. (2017) reported in the Space Environmental Data Acquisition Monitor onboard the Himawari-8 satellite during a magnetic storm on March 17–20, 2015). In Nagatsuma et al. (2017), SEDA Channels 6 (2 MeV) and 7 (4.5 MeV) showed different phases of diurnal variability compared to the lower channels prior to storm arrival, with Channel 6 (2 MeV) occasionally showing larger fluxes than channel 5 (1.5 MeV). Nagatsuma et al. (2017) suggested that residuals of the bias current, resulting from the daily fluctuation in sensor temperature, could be the cause of this phase variations. Further analysis is needed to determine whether this is also applicable to KSEM PD. If applicable, it seems plausible that additional post-processing could be employed for correction in the future.

Case 2: June 13–June 26

On June 15, 2021, an HSS of 620 km/s was detected by DSCOVR at L1. HSSs arrived at Earth at the end of the day. KSEM PD and MPS-HI observed similar trends during the HSSs, with dropouts observed immediately after arrival. Prior to the HSS, Channel 9 of the KSEM PD showed different phase daily flux variations, similar to the April event. After the HSS, the flux levels of Channels

8–9 from the KSEM PD were reversed, compared with the pre-HSS levels.

Case 3: October 27–November 13

On October 28, an X-class flare occurred with an accompanying solar energetic particle event (SPE). Energetic electrons from SEPs have limited penetration into the Earth's magnetosphere, and Zhang et al. (2022) also reported no significant enhancement for MeV electrons at geostationary orbit. However, it is noteworthy that Xiao et al. (2005) also reported detections of increased electron flux enhancements of 100 s keV electrons in the magnetosphere during some SEPs. Subsequently, on November 9, a long-duration solar flare event occurred.

On October 30–November 1, the lower energy electron flux measured by KSEM PD (< 1350 keV, Channels 2–6) showed an increase and fluctuations, with weak flux dropouts at 325–1350 keV preceding the increase. Higher energy electron flux (> 1350 keV, Channels 7–9) was enhanced 1–3 days later. MPS-HI showed similar delayed increases in higher energy electron flux, with more prominent flux dropouts across a broader energy range (< 1360 keV). A halo-coronal mass ejection directed toward Earth occurred on November 2, and its effects were observed on November 3 by two instruments with significant fluctuations in flux. Please note that during SPEs, there is a high probability of proton contamination in electron detectors. However, assessing the effect of this contamination is challenging with the current dataset, especially considering that SPEs are sometimes accompanied by increases in electron flux below 10 MeV, as mentioned above.

During the enhanced particle events, the measurements from both detectors showed similar trends, with MPS-HI demonstrating higher fluctuations and more robust responses. The amplitude differences might be due to differences in instrument response function and calibration method and/or due to natural dynamics of energetic electrons. Further analysis of the detailed differences between the two instruments and in-depth analysis of electron dynamics will be necessary for clarification.

Summary and discussion

This study compared the energetic electron differential fluxes measured by GK2A KSEM PD and GOES-16 MPS-HI. The electron flux data from the two detectors showed good correspondence and a strong correlation (R-values over 0.8). Both flux-energy spectra showed good agreement, with similar spectral shapes, except for the energy level < 225 keV (Channel 2) and > 2600 keV (Channel 9). We plan to improve the Channel 9 data by incorporating a procedure that uses its proton fluxes to estimate fluxes in higher energy bands, thereby reducing background noise. In particular, the upcoming KSEM-II, designed for future satellites, will include a dedicated sensor to address proton contamination. As for the slightly lower values in KSEM PD's low-energy channels, we do not currently have enough data to definitively determine the cause. However, with continued analysis and expanded data collection, we aim to increase our understanding of both the data and their background dynamics, and to continuously improve the data processing system.

The quarterly variations of the flux distribution were less significant in 2021 than in 2020, which may be due to the end of the solar cycle minimum. The monthly correlation coefficients showed mostly reasonable correlations. Notable decreases in R and α values were observed above channel 7 during certain months. However, these decreases hold no significance as they result from the absence of significant flux variation from both sensors within those energy bands at those times. Although MPS-HI measurements for three selected cases of flux enhancement events showed more robust responses than the KSEM PD observations, the key features and overall flux variation trends were very similar between the two detectors. Further long-term analysis is needed to study and understand the asymmetric distribution and dynamics of energetic particles in the GEO. Additional analysis to calibrate and improve data quality for the energy level > 2600 keV is indispensable because energetic electrons with energy above 2 MeV is also one of critical factors affecting the safety of satellites (Iucci et al. 2005; Forsyth et al. 2020; Sun et al. 2021). Combining the magnetic field data from each satellite's magnetometers will help to understand the electron flux characteristics found in this study. The focus here is primarily on the comparison using omnidirectional fluxes; more detailed analysis considering pitch angles and magnetic fields is needed in subsequent research.

The results of this study show the usefulness of GK2A KSEM PD data in monitoring the energetic electron environment in the eastern hemisphere, and potential for multi-point in situ-based space weather monitoring when combined with data from MPS-HI onboard the GOES-R satellite series in the western hemisphere. Characteristic differences between the data from the two detectors, separated by half a day in local time, demonstrate the importance of multi-point measurements in determining energetic flux distributions at different locations. This allows a more detailed understanding of location-dependent differences during active space weather environments. The space weather effects on spacecraft in different orbits could vary significantly (Iucci et al. 2005; Lu et al. 2019), and even at the geostationary orbit, the space weather environment is asymmetric and dynamically responsive (Wing and Sibeck 1997; Sanny et al.

2002; Lee and Lyons 2004; Borodkova et al. 2008; Dong et al. 2014). Thus, reliable multi-point in situ data from multiple satellites, such as GOES, Himawari-8 and -9, EDRS-C, and FY satellites, are needed to provide more precise energetic particle distributions and support advanced now/forecasting models. Improving cross-satellite analysis of particle distributions in Earth's magnetosphere is critical for obtaining accurate and consistent in situ particle measurements, advancing our understanding of space weather phenomena, and the ability to forecast enhanced particle events that may impact assets in space.

Abbreviations

GEO	Geostationary Earth orbit
NOAA	National Oceanic and Atmospheric Administration
GOES	Geostationary Operational Environmental Satellite
SEM	Space Environment Monitor
FY	Fengyun
GK2A	GEO-KOMPSAT-2A
KSEM	Korean space weather monitor
PD	Particle detector
MPS-HI	Magnetosphere Particle Sensor–High
HSS	High-speed solar wind stream
SPE	Solar proton event

Supplementary Information

The online version contains supplementary material available at https://doi.org/10.1186/s40623-024-01992-y.

Additional file 1. Local times of GK2A KSEM and GOES-16 MPS-HI when the conjunction conditions were satisfied.

Additional file 2. The number of data points satisfying the conjunction conditions during a day for calculating the daily average flux.

Acknowledgements
We would like to thank Editage (www.editage.com) for their assistance with English language editing. We extend our sincere appreciation to the two anonymous reviewers and the journal's editors, including the editor-in-chief Prof. T. Sagiya, for their constructive comments that significantly contributed to the enhancement of this manuscript.

Author contributions
DO performed statistical analysis for this study and drafted the manuscript. JK, PL, HL, DL, and DK discussed the results and edited the manuscript. All authors read and approved the final manuscript.

Funding
This research was supported by the "Technical development for improving space weather data quality and data application service" (KMA2020-00125) of "Technical Development on Weather Forecast Support and Convergence Service using Meteorological Satellites" project funded by the National Meteorological Satellite Center, Korea Meteorological Administration.

Availability of data and materials
The data analyzed during the study are available from the corresponding author on reasonable request. The original data used during the study are available on following web pages. GK2A data: http://datasvc.nmsc.kma.go.kr/datasvc/html/main/main.do?lang=en. GOES-16 data: https://www.ngdc.noaa.gov/stp/satellite/goes-r.html. DSCOVR data: https://www.ngdc.noaa.gov/dscovr/portal/. Kp index data: https://www.gfz-potsdam.de/en/section/geomagnetism/data-products-services/geomagnetic-kp-index. Dst index data: https://wdc.kugi.kyoto-u.ac.jp/dstdir/

Declarations

Ethics approval and consent to participate
Not applicable.

Consent for publication
Not applicable.

Competing interests
The authors declare that they have no competing interests.

Author details
[1]National Meteorological Satellite Center, Korea Meteorological Administration, Jincheon, Chungcheongbuk-do, Republic of Korea. [2]Cooperative Institute for Research in Environmental Sciences, University of Colorado Boulder, Boulder, CO, USA. [3]National Centers for Environmental Information, National Oceanic and Atmospheric Administration, Boulder, CO, USA. [4]Chungbuk National University, Cheongju-si, Chungcheongbuk-do, Republic of Korea.

Received: 13 March 2023 Accepted: 8 March 2024
Published online: 22 March 2024

References

Baker DN (2001) Space storms and space weather hazards. In: Daglis IA (ed) Satellite anomalies due to space storms. Springer, Netherlands, Dordrecht, p 285–311

Bessho K, Date K, Hayashi M, Ikeda A, Imai T, Inoue H et al (2016) An introduction to himawari-8/9— Japan's new-generation geostationary meteorological satellites. J Meteorol Soc Jpn Ser Ii 94:151–183. https://doi.org/10.2151/jmsj.2016-009

Borodkova NL, Liu JB, Huang ZH, Zastenker GN (2008) Geosynchronous magnetic field response to the large and fast solar wind dynamic pressure change. Adv Space Res-Ser 41:1220–1225. https://doi.org/10.1016/j.asr.2007.05.075

Boudouridis A, Rodriguez JV, Kress BT, Dichter BK, Onsager TG (2020) Development of a bowtie inversion technique for real-time processing of the GOES-16/-17 SEISS MPS-HI electron channels. Adv Space Res. https://doi.org/10.1029/2019sw002403

Burrell AG, Halford A, Klenzing J, Stoneback RA, Morley SK, Annex AM et al (2018) Snakes on a spaceship—an overview of python in heliophysics. J Geophys Res Space Phys 123:10384–10402. https://doi.org/10.1029/2018ja025877

Choi HS, Lee J, Cho KS, Kwak YS, Cho IH, Park YD et al (2011) Analysis of GEO spacecraft anomalies: space weather relationships. Adv Space Res. https://doi.org/10.1029/2010sw000597

Dichter BK, Galica GE, McGarity JO, Tsui S, Golightly MJ, Lopate C et al (2015) Specification, design, and calibration of the space weather suite of instruments on the NOAA GOES-R program spacecraft. IEEE T NuclSci 62:2776–2783. https://doi.org/10.1109/tns.2015.2477997

Dong YX, Cao JB, Liu WL, Zhang L, Li LY (2014) Response of magnetic fields at geosynchronous orbit and on the ground to the sudden changes of IMF BZ. Sci China Technol Sci 57:360–367. https://doi.org/10.1007/s11431-013-5428-6

Ferguson D, Denig W, Rodriguez J (2011) Plasma Conditions During the Galaxy 15 Anomaly and the Possibility of ESD from Subsurface Charging. 49th AiaaAerospSci Meet Incl New Horizons Forum Aerosp Expo. https://doi.org/10.2514/6.2011-1061

Forsyth C, Watt CEJ, Mooney MK, Rae IJ, Walton SD, Horne RB et al (2020) Forecasting GOES 15 >2 MeV electron fluxes from solar wind data and geomagnetic indices. Adv Space Res. https://doi.org/10.1029/2019sw002416

Galica GE, Ditcher BK, Tsui S, Golightly MJ, Lopate C, Connell JJ (2016) GOES-R space environment in-situ suite: instruments overview, calibration results, and data processing algorithms, and expected on-orbit performance. Earth Obs Mission Sens Dev Implement Charact. https://doi.org/10.1117/12.2228537

Iucci N, Levitin AE, Belov AV, Eroshenko EA, Ptitsyna NG, Villoresi G et al (2005) Space weather conditions and spacecraft anomalies in different orbits. Adv Space Res. https://doi.org/10.1029/2003sw000056
Larson DE, Lillis RJ, Lee CO, Dunn PA, Hatch K, Robinson M et al (2015) The MAVEN solar energetic particle investigation. Space Sci Rev 195:153–172. https://doi.org/10.1007/s11214-015-0218-z
Lee DY, Lyons LR (2004) Geosynchronous magnetic field response to solar wind dynamic pressure pulse. J Geophys Res Space Phys. https://doi.org/10.1029/2003ja010076
Lin RP, Anderson KA, Ashford S, Carlson C, Curtis D, Ergun R et al (1995) A three-dimensional plasma and energetic particle investigation for the wind spacecraft. Space Sci Rev 71:125–153. https://doi.org/10.1007/bf00751328
Lohmeyer WQ, Cahoy K (2013) Space weather radiation effects on geostationary satellite solid-state power amplifiers. Adv Space Res 11:476–488. https://doi.org/10.1002/swe.20071
Loto'aniu TM, Singer HJ, Rodriguez JV, Green J, Denig W, Bieseckere D et al (2015) Space weather conditions during the galaxy 15 spacecraft anomaly. Adv Space Res 13:484–502. https://doi.org/10.1002/2015sw001239
Lu Y, Shao Q, Yue H, Yang F (2019) A review of the space environment effects on spacecraft in different orbits. Ieee Access 7:93473–93488. https://doi.org/10.1109/access.2019.2927811
Luhmann JG, Curtis DW, Lin RP, Larson D, Schroeder P, Cummings A et al (2005) IMPACT: science goals and firsts with STEREO. Adv Space Res-Ser 36:1534–1543. https://doi.org/10.1016/j.asr.2005.03.033
Magnes W, Hillenmaier O, Auster H-U, Brown P, Kraft S, Seon J et al (2020) Space weather magnetometer aboard GEO-KOMPSAT-2A. Space Sci Rev 216:119. https://doi.org/10.1007/s11214-020-00742-2
Morley SK, Niehof JT, Welling DT, Larsen BA, Brunet A, Engel MA et al (2022) SpacePy. Zenodo. https://doi.org/10.5281/zenodo.7083375
Nagatsuma T, Sakaguchi K, Kubo Y, Belgraver P, Chastellain F, Muff R et al (2017) Space environment data acquisition monitor onboard Himawari-8 for space environment monitoring on the Japanese meridian of geostationary orbit. Earth Planets Space 69:75. https://doi.org/10.1186/s40623-017-0659-6
NASA (2011) Mitigating in-space charging effects—a guideline (NASA Technical Handbook NASA-HDBK-4002A). National Aeronautics and Space Administration, Washington, DC
Oh D, Kim J, Lee H, Jang K-I (2018) Satellite-based in-situ monitoring of space weather_ KSEM mission and data application. J Astron Space Sci. https://doi.org/10.5140/jass.2018.35.3.175
Sakaguchi K, Nagatsuma T (2022) Impact of space environment on geostationary meteorological satellite data outage. Space Weather. https://doi.org/10.1029/2021SW002965
Sandberg I, Aminalragia-Giamini S, Papadimitriou C, Van Gijlswijk R, Heynderickx D, Marcinkowski R et al (2022) First results and analysis from ESA next generation radiation monitor unit onboard EDRS-C. IEEE Trans Nucl Sci 69:1549–1556. https://doi.org/10.1109/TNS.2022.3160108
Sanny J, Tapia JA, Sibeck DG, Moldwin MB (2002) Quiet time variability of the geosynchronous magnetic field and its response to the solar wind. J Geophys Res Space Phys. https://doi.org/10.1029/2002ja009448
Seon J, Chae K-S, Na GW, Seo HK, Shin YC, Woo J et al (2020) Particle detector (PD) experiment of the Korea space environment monitor (KSEM) aboard geostationary satellite GK2A. Space Sci Rev 216:13. https://doi.org/10.1007/s11214-020-0636-4
Sibeck DG, Angelopoulos V (2008) THEMIS science objectives and mission phases. Space Sci Rev 141:35–59. https://doi.org/10.1007/s11214-008-9393-5
Sun X, Lin R, Liu S, He X, Shi L, Luo B et al (2021) Modeling the relationship of ≥2 MeV electron fluxes at different longitudes in geostationary orbit by the machine learning method. Remote Sens-Basel 13:3347. https://doi.org/10.3390/rs13173347
Van Allen JA, Ludwig GH, Ray EC, McIlwain CE (1958) Observation of high intensity radiation by satellites 1958 alpha and gamma. J Jet Propuls 28:588–592. https://doi.org/10.2514/8.7396
Wing S, Sibeck DG (1997) Effects of interplanetary magnetic field z component and the solar wind dynamic pressure on the geosynchronous magnetic field. J Geophys Res Space Phys 102:7207–7216. https://doi.org/10.1029/97ja00150
Woo J, Seol WH, Chae KS, Lee JH, Lee ES, Seon J (2020) Charging monitor aboard the geostationary satellite GK2A at 128.2° E longitude. Ieee T NuclSci 67:740–745. https://doi.org/10.1109/tns.2020.2977473
Xiao CJ, Pu ZY, Chen HF, Xie L, Zong QG, Fritz TA, Daly PW (2005) Energetic electrons in magnetosphere during gradual solar energetic particle event observations by cluster. Proc Int Astron Union 2004(IAUS226):473–474. https://doi.org/10.1017/S1743921305001080
Yang J, Zhang Z, Wei C, Lu F, Guo Q (2016) Introducing the new generation of Chinese geostationary weather satellites—FengYun 4 (FY-4). B Am MeteorolSoc 98:1637–1658. https://doi.org/10.1175/bams-d-16-0065.1
Zhang Y, Ni B, Xiang Z, Zhang X, Zhang X, Gu X et al (2018) Inter-satellite calibration of FengYun 3 medium energy electron fluxes with POES electron measurements. Adv Space Res-Ser 61:2290–2300. https://doi.org/10.1016/j.asr.2018.02.017
Zhang Z, Li X, Wang L, Zhima Z, Shen X, Yuan S et al (2022) Evaluation of the proton contamination to MeV electrons by solar proton events based on CSES observations. J Geophys Res: Space Phys. https://doi.org/10.1029/2022JA030550

Publisher's Note